Multi-Nutrient Deficiency Identification via Improved LinkNet-SqueezeNet Model and Improved BIRCH based Segmentation

[*1,2]Kavitha S., and [3]Kotadi Chinnaiah

Abstract- Multi-nutrient deficiencies in rice paddy plant leaves including nitrogen, phosphorus, and potassium shortages, manifest symptoms like discolouration and stunted growth. Conventional identification methods, relying on visual inspection, are time-consuming, subjective, and prone to errors. Advanced models via Machine Learning (ML) and Deep Learning (DL) offer higher accuracy and efficiency but require significant computational resources and high-quality training data. This research proposed a new Multi-Nutrient Deficiency Identification model via Improved LinkNet and SqueezeNet (ILink-SqueezeNet). The model follows a structured methodology that includes preprocessing, segmentation, feature extraction, and identification. At first, the input paddy leaf image undergoes enhancement through Gaussian filtering to refine its quality. The preprocessed image is then segmented using an Improved Balanced Iterative Reducing and Clustering using Hierarchies (I-BIRCH) method. After segmentation, the crucial features like color features, Hierarchy of skeleton-based features and improved MRE-LBP-based features are retrieved from the segmented image. These features are then analysed by the ILink-SqueezeNet model, which identifies nutrient deficiencies in the paddy leaf. Eventually, comprehensive simulations and experimental calculations are shown to assess and validate the efficiency and robustness of the proposed ILink-SqueezeNet model. Therefore, the research outperforms the potential of the ILink-SqueezeNet model to expressively advance nutrient deficiency detection in agricultural applications.

Keywords: Multi-Nutrient Deficiency Identification, Paddy leaf, I-BIRCH, Improved LinkNet, and MRE-LBP based feature.

1. Introduction

Agriculture plays a crucial role in the global economy and food security, facing pressure due to rapid population growth [9] [19] [24]. The growth of plants and crops heavily relies on various nutrients, with 14 essential mineral elements necessary for their life cycle [23][18]. These nutrients are vital for overall plant growth and development [7]. Rice, the most widely cultivated food crop globally, serves as a staple for half of the world's population [1] [5] [11]. It holds paramount importance in feeding a significant portion of humanity [4] [15]. India stands as one of the top two agricultural producers globally, with agriculture deeply embedded in its economy [1].

Rice necessitates sixteen nutrients for optimal growth, including primary macronutrients such as N, P, and K, secondary macronutrients like Mg, Ca, and S, and micronutrients including Zn, Fe, Mn, Cu, B, Mo, and Cl. Among these, nitrogen (N), phosphorus (P), and potassium (K) stand out as the most critical for plant health and development [4][14].

Manual observation for identifying nutrient deficiencies in paddy has several drawbacks while significant advancements in machine learning, deep learning, and image processing techniques, offers promising avenues for the creation of rapid, real-time tools capable of analyzing images captured with high-resolution, multi-featured cameras [16] [22] [21] [20] [25] [3] [10] [6]. The suggested model proposes a frame for the identification of nutrient deficiency in paddy with three contributions, which are methodically elaborated upon as follows.

▪ Introducing an enhancement in the segmentation stage, referred to as I-BIRCH. This improvement is achieved through automated threshold initialization, which dynamically adjusts the threshold value based on mutual information. This process results in more accurate and predictive clustering compared to static thresholds.

▪ Retrieving an enhanced feature along with precise vital features during the retrieval of the feature stage from the segmented image. This enhanced feature named Improved MRE-LBP, boosts the descriptor's ability to differentiate between various textures in the image, leading to better identification performance.

▪ Presenting a hybrid model that incorporates the ILink-SqueezeNet model, which is enhanced by the ReLU activation function in the Improved LinkNet model. This enhancement ensures that the proposed model's gradients do not vanish as quickly as with traditional activation functions, leading to faster convergence during training and more efficient learning.

[1*]*Research Scholar Computer Science & Engineering G. H Raisoni University, Amravati, Maharashtra -444701,India.*

[1*]*kavithabhavana@gmail.com*

[2]*Assistant Professor School of Computer Engineering MIT Academy of Engineering, Pune, Maharashtra -412105,India.*

[3] *Associate Professor Computer Science and Engineering G. H. Raisoni College of Engineering, Nagpur, Maharashtra, 440016,India.*

2. Literature Review

In this section, a succinct overview of nutrient deficiency identification is provided by integrating insights from pertinent research papers.

In 2024, Fubing Liao *et al.,* [2] implemented a hybrid model for diagnosing rice nutrient levels at the EPIS which combined a CNN with an attention mechanism and an LSTM network. Therefore, the model was validated using a substantial collection of sequential images of rice canopies captured by a UAV across different growth stages during a two-year experiment. When compared to GoogleNet, InceptionV3, AlexNet, ResNet101, VGG16, and DenseNet the model combined with LSTM achieved the highest accuracy of 83.81% on the Huanghuazhan dataset.

In 2023, Anshuman Nayak *et al.,* [3] developed a new MobileNetV2 model to detect plant disease with high accuracy. This model utilized 2259 smartphone images of various parts of rice plants, capturing different classes of data to classify 12 rice diseases and nutrient deficiency symptoms. To ensure accuracy, 250 real-time validation images were employed. Various image segmentation techniques, such as foreground extraction, were implemented to isolate the affected portions of the plants. The resulting model was then integrated into an Android application named "Rice Disease Detector." This application, powered by the MobileNetV2 model, was rigorously tested for its ability to identify multiple disease occurrences in a single capture.

In 2023, Md. Simul Hasan Talukder and Ajay Krishno Sarkar [4] suggested a robust DECNN model capable of diagnosing rice nutrient deficiency with high accuracy. Modified DenseNet169 model achieved the accuracy of 96.66%.

In 2024, Shrikrishna Kolhar *et al.,* [7] presented an image-based DL framework for nutrient deficiency identification with Xception model, vision transformer, and MLP mixer model, were trained to identify N, P and K deficiencies in rice plants from RGB images. Ultimately, the framework performance was evaluated via publicly available dataset on Kaggle and gave 92% accuracy.

In 2022, Amrute Chore and Dolly Thankachan [8] introduced a nonintrusive multifrequency visible light analysis framework for identifying multiple nutrient deficiencies across a wide variety of plants. With extensive learning, the framework accurately mapped spatial and temporal light properties to nutrient shortages.

This paper proposes a new deep-learning model for identifying nutrient deficiency in paddy leaf images, with the goal of overcoming the limitations presented in conventional models.

3. Outline the proposed Multi-Nutrient Deficiency Identification via ILink-SqueezeNet model

Nutrient deficiency in rice paddy leaves can negatively impact plant health and crop yield. Identifying these deficiencies accurately is crucial for effective management. Advanced models using machine learning and deep learning can detect and classify these deficiencies, but their interpretability may hinder decision-making by farmers and agronomists.

This research proposes a DL-based approach for identifying nutrient deficiencies in paddy leaves using the ILink-SqueezeNet model. The procedure begins with the preprocessing stage, where the input paddy leaf image is enhanced using a Gaussian filtering technique to improve its quality. Next, the preprocessed image enters the segmentation stage, where the deficiency portions are segmented through an I-BIRCH based segmentation process. This segmentation segments the areas of the leaf that are potentially deficient in nutrients. The segmented image then undergoes feature extraction to retrieve relevant features. This involves retrieving color features, features from the hierarchy of skeletons, and MRE-LBP based features from the segmented image. These features are crucial for accurately identifying nutrient deficiencies. Finally, these retrieved features are processed through the identification stage using the ILink-SqueezeNet model. This model employs the detailed features to recognize and classify the specific nutrient deficiencies in the paddy leaf. The overall framework for identifying nutrient deficienc through paddy leaf images is illustrated in Figure 1
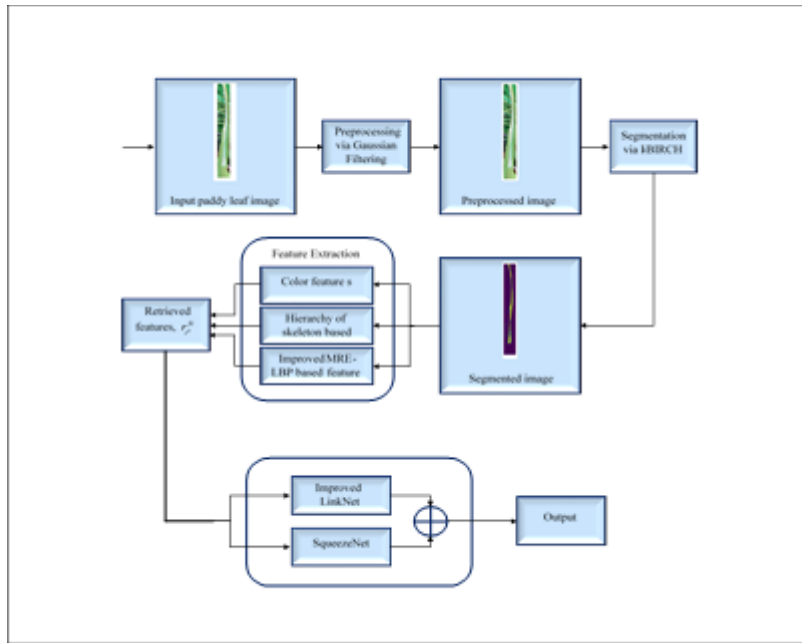
Fig 1: Overall architecture of the ILink-SqueezeNet model based Multi-Nutrient Deficiency Identification

3.1. Preprocessing using Gaussian Filtering

The input image i^p is subject to preprocessing stage to improve the image quality. In this ILink-SqueezeNet model, Gaussian filtering technique is employed in this preprocessing stage.

The general Equation for Gaussian filter is represented in Eq. (1).

$$Gaussian(r,s) = \frac{1}{2\pi St^2} e^{-\frac{r^2+s^2}{2St^2}}$$

(1)

From Eq. (1), (r,s) implies the coordinates which is relative to the kernel center, gaussian function value is represented by $Gaussian(r,s)$ at coordinates (r,s), and the value of establishes the kernel width, acting as the standard deviation St for the Gaussian distribution. Thereby, the input paddy leaf image is enhanced by Gaussian filtering technique and its output is indicated as,

p^{i^p} (i.e. preprocessed image).

3.2. Improved BIRCH based Segmentation

The I-BIRCH algorithm, proposed in the ILink-SqueezeNet model, aims to optimize the segmentation of preprocessed images for identifying multi-nutrient deficiencies by implementing four distinct stages, with one stage enhancing its efficacy A thorough illustration of the flow of the proposed I-BIRCH algorithm is presented in **Figure 2.**
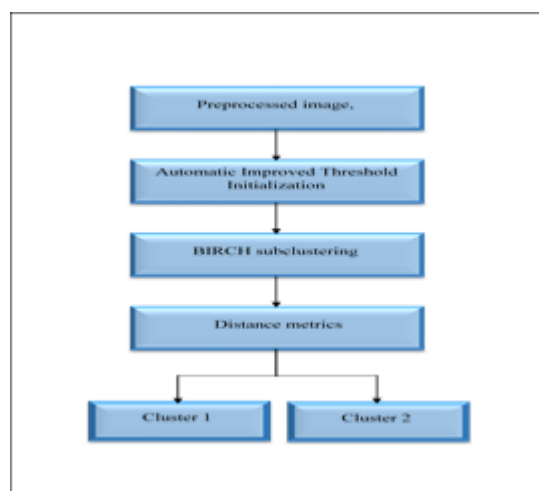

Fig 2: Framework of proposed I-BIRCH based segmentation

1) Preprocessing the preprocessed image- In this I-BIRCH algorithm, the preprocessed image p^{i^p} undergoes further preprocessing. Essential features relevant to classification are chosen, mapped to appropriate labels of the cluster and any detected outliers are removed through feature rescaling.

2) Automatic Improved Threshold Initialization- The mathematical calculation for conventional automatic threshold initialization via mutual information [27] is given in Eq. (2).

$$MI = \sum_{a,b} \mathrm{P}(a,b) \log \frac{\mathrm{P}(a,b)}{\mathrm{P}(a)\mathrm{P}(b)}$$

(2)

In Eq. (2), a and b signifies the image and mask inputs, the function $\mathrm{P}(a,b)$ signifies the joint probability distribution of variables A and B, while $\mathrm{P}(a)$ and $\mathrm{P}(b)$ denote the marginal probability distribution functions for A and B, respectively. But the conventional threshold initialization poses a risk of suboptimal clustering attributed to improper parameter settings. So, an enhanced method utilizing improved mutual information for automatic threshold initialization, as defined in Eq (3), is proposed. This enhancement dynamically adjusts the threshold value based on Mutual Information, resulting in more precise cluster results compared to employing a static threshold. With automatic threshold initialization, the process becomes less reliant on manual tuning, thereby mitigating the risk of suboptimal clustering due to improper parameter settings.

$$MI_{new} = \left[\frac{MI(a,b) * \frac{\mathrm{H}(a)*\mathrm{H}(b)}{\mathrm{H}(a)+\mathrm{H}(b)}}{\frac{1}{2}\left[(\mathrm{H}(a)+\mathrm{H}(b)*\exp\mathrm{H}(b))\right]} \right]$$

(3)

In Eq. (3), the term

$$\mathrm{H}(a) = \left\{ \frac{-\sum_{F_e \subseteq \theta} m(F_e) \log_2 \left(\frac{m(F_e)}{2^{|F_e|-1}} * e^{\frac{|F_e|-1}{|S|}} \right)}{\left[1 + e^{-\left(\log_2 \frac{m(F_e)}{|F_e|-1} \right)} \right]} \right\},$$

$$\mathrm{H}(b) = -\sum_{i=1}^{N} \mathrm{P}(a_i) \log_b \mathrm{P}(a_i) \text{ at } b = 2, \; F_e \text{ implies}$$

the focal element and $|F_e|$ represents the focal element cardinality.

3) Birch sub clustering- During this sub-clustering phase, individual data point encapsulating diverse features pertaining to nutrient levels, symptoms, and medical history of individuals undergoes allocation to a sub-cluster contingent upon its likeness to the centroid of that sub-cluster. This similarity is typically evaluated utilizing distance metrics like cosine similarity or Euclidean distance. By iteratively assigning data points to their nearest sub-cluster centroid, the algorithm incrementally refines segmentation, methodically disassembling larger, amalgamated clusters of multi-nutrient deficiency cases into more refined, coherent groups.

4) Altering Distance metrices in the baseline birch- In the fourth step of the BIRCH algorithm, which focuses on altering distance metrics, adaptation for multi-nutrient deficiency identification involves a critical shift. Thus, the distance [28] is calculated by Eq. (4).

$$Dist = \sum_{i=1}^{n} \min\left(|c_i - d_i|, q - |c_i - d_i|\right)$$

(4)

In Eq. (4), c_i, d_i signify the pixels which are adjacent to one another.

In the final stage of I-BIRCH, the algorithm produces clusters, characteristically labelled as Cluster 1, Cluster 2, and so forth, representing the dataset's segmented partitions based on the clustering process. Once these clusters are derived, the segmented image can be constructed by associating individual pixel in the original image with its corresponding cluster. This pixel-to-cluster assignment relies on the clustering outcomes generated by the I-BIRCH algorithm. Individual cluster delineates a set of pixels within the image that share similar features. Therefore, the resulting segmentation image obtained through I-BIRCH is indicated as, s^{i^p}.

3.3. Feature Extraction

After preprocessing, the segmented image s^{i^p} enters a crucial phase called feature extraction. Here, the segmented image s^{i^p} is carefully analyzed to measure important characteristics necessary for identification. The main goal is to pinpoint unique attributes within the image like color features, hierarchy of skeleton-based features, and Improved MRE-LBP-based features that aid in accurately identifying nutrient deficiencies.

3.3.1. Color features

When examining segmented image s^{i^p}, utilizing color features such as color histograms offers significant understandings into the attributes and distribution of pixel intensities in the segmented areas. In this context, the process entails taking the segmented image s^{i^p} as input to retrieve and analyze the color features.

Color Histogram: It displays the pixel intensities distribution in the segmented area across several color channels. It illustrates the prevalence of each intensity level, offering a comprehensive perspective of the color distribution [29], as given in Eq. (5).

$$Co^{Histogram} = \left\{ h_i[C_1], h_i[Co_{12}], \ldots, h_i[Co_k] = 1, 0 \le h_i[Co_k] \le 1 \right\}$$

(5)

The frequency of the pixel is represented as $h_i[Co_k]$ indicating the occurrence of a particular kth color within the image is expressed in Eq. (6).

$$h_i[Co_k] = \frac{\sum_{i=0}^{Wi_1-1} \sum_{j=0}^{Wi_2-1} \begin{cases} 1\left(s^{i^p}(i,j) = Co_k\right) \\ 0(other) \end{cases}}{Wi_1 \times Wi_2}$$

(6)

From Eq. (6), the variable representing the width of the image is indicated by Wi_1 while the height of the image is represented as Wi_2. Therefore, the output obtained from this stage is implied as, $Color^{fe}$.

3.3.2. Hierarchy of Skeleton based features

This proposed model efficiently operates on retrieving the hierarchical skeleton-based features via segmented image, s^{i^p}. In essence, skeleton shapes are a category of geometric models that highlight the medial axis of an image shape [30]. They essentially represent the structural shape of an object within an image, outlining the spatial arrangement of contours and component parts. These axes within shapes are organized hierarchically, delineating the overall coarse geometry of a shape through a series of parent axes, while smaller offshoot axes detail specific component parts [19]. Hence, the feature retrieved from the segmented image, s^{i^p} is denoted as HS^{fe}.

3.3.3. Improved MRE-LBP based feature

MRE-LBP [31] is an enhanced version of the LBP technique used for texture analysis. MRE-LBP integrates a median filter with multiresolution support, employing median values from local patches instead of raw pixel values. The approach begins by replacing the values of the pixel at specific locations with representative values averaged over an area. MRE-LBP variations based on CI, NI and RD deliver superior texture classification performance. These variations capture information about intensity of the central pixel's, intensity of the neighboring pixel's, and radial differences, respectively.

Mathematically, the conventional center intensity-based MRE-LBP is represented by an equation (Eq. 7), where $Z^{c,t}$ denotes a local patch centered at pixel z^c at size $t \times t$, $\phi(Z)$ signifies the value of median over the patch, Z and μ^t denotes the average value of the image's pixel intensities $\phi(Z^{c,t})$.

$$MRELBP - CI(z^c) = m(\phi(Z^{c,t}) - \mu^t)$$

(7)

But the conventional center intensity based MRE-LBP cause more sensitive to outliers, which leads to poor performance especially in noisy image conditions. To overcome this challenge, modifications have been made to how the center pixel is represented. This improved method is mathematically formulated in Eq. (8), where μ^t denotes the mean value of $\phi(Z^{c,t})$ across the entire image. The calculation of conventional $\phi(Z^{c,t})$ is illustrated in Eq. (9), G_s, B_s and M_s represents the image and various smoothing techniques such as bilateral smoothing, Gaussian smoothing, and median smoothing are applied respectively. The estimation of μ^t involves averaging the interquartile mean and contraharmonic mean, as expressed in Eq. (11),

The modified center intensity-based MRE-LBP method enhances descriptor performance by incorporating local texture information, improving classification tasks, and reducing outlier sensitivity compared to conventional average filters.

In instances where the image is afflicted by noise, the refined filtering approach demonstrates its effectiveness by substantially reducing noise levels when contrasted with solely employing a median filter. Additionally, it is adept at preserving the fine details and edges within the image, ensuring that important visual information remains intact.

$$IMRELBP - CI(z^c) = \frac{S(\phi(Z^{c,t}) - \mu^t)}{\sqrt{\phi(Z^{c,t})} * 1 + e^{-(X^{c,t})}}$$

(8)

$$\phi(Z^{c,t}) = (Gaussian + Bilateral)/2$$

(9)

Thus, the proposed median filter is given in Eq. (10)

$$\phi(Z^{c,t})_{new} = Median * \phi(Z^{c,t})$$

$$(10)$$

$$mean = \left[Intraquartile\, mean + contra\, harmonic\, mean\right]$$

$$(11)$$

The neighborhood intensity based improved MRE-LBP as delineated in Eq. (12), involves the utilization of a patch centered around the neighboring pixel $z^{r,l,d}$, where $Z^{r,l,t_r,d}$ denotes the size of the patch approximately equal to $t_r \times t_r$.

$$MRELBP - NI^{r,l}(z^c) = \sum_{d=0}^{l-1} m(\phi(Z^{r,l,t_r,d}) - \mu^{r,l,t_r})2^d$$

$$(12)$$

here $\mu^{r,l,t_r} = \dfrac{1}{l}\sum_{d=0}^{l-1}\phi(Z^{r,l,t_r,d})$. Then the formulation of the MRE-LBP based radial difference is represented in Eq. (13), where $Z^{r,l,t_r,d}$ and $Z^{r-1,l,t_{r-1},d}$ denote patches centered at nearby pixels $z^{r,l,d}$ and $z^{r-1,l,d}$ respectively. Here, $\left\{z^{r,l,d}\right\}_{d=0}^{l}$ signifies the center pixel neighbors z^c, organized uniformly and circularly spaced at a radius r. Additionally, the inclusion of the improved median filter $\phi()$ further strengthens the robustness of the representation against noise.

$$MRELBP - RD^{r,r-1,l,t_r,t_{r-1}},(x^c) = \sum_{d=0}^{l-1} m(\phi(Z^{r,l,t_r,d}) - \phi(Z^{r-1,l,t_{r-1},d}$$

$$(13)$$

So, the outcome derived from this improved MRE-LBP based feature is indicated as $MRE - LBP^{fe}$. Finally, the pertinent characteristics such as color features $Color^{fe}$, the hierarchy of skeleton-based features HS^{fe}, and the improved MRE-LBP based feature $MRE - LBP^{fe}$ are retrieved. As a result, these retrieved features are totally denoted as $r_{i^p}^{fe}$.

3.4. Hybrid Model based Nutrient Deficiency Identification: Combining Improved Linknet and Squeezenet Architecture

Identifying multi-nutrient deficiencies is a crucial step within the proposed ILink-SqueezeNet framework. The retrieved features $r_{i^p}^{fe}$ play a pivotal role as they are utilized to discern nutrient deficiencies in paddy leaves. To address this objective, a pioneering hybrid model termed ILink-SqueezeNet is introduced. This innovative model merges the Improved LinkNet and SqueezeNet, as illustrated in **Figure 3,** presenting a new approach to nutrient deficiency identification. The forthcoming sections will delve into comprehensive explanations of both classifiers, elucidating their roles and functionalities within the framework.
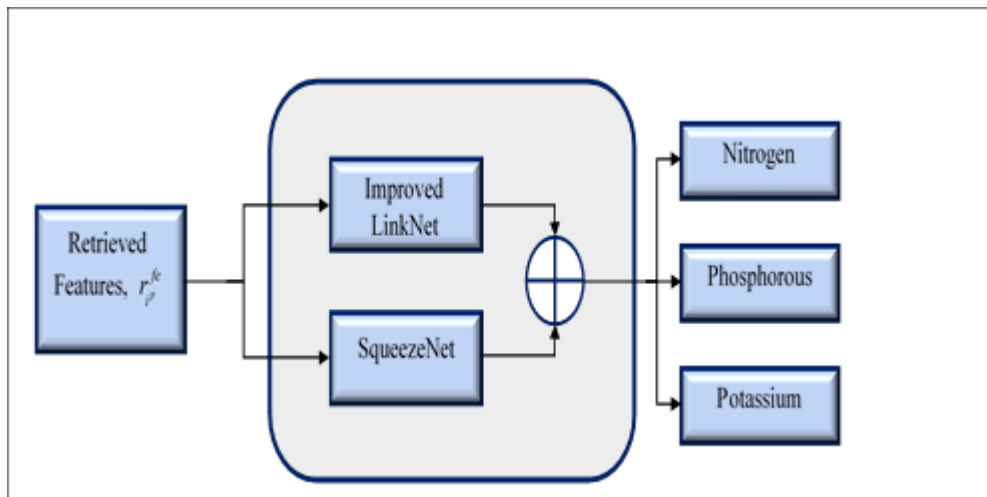

Fig 3: Multi-Nutrient Deficiency Identification via ILink-SqueezeNet

3.4.1. Improved LinkNet

Improved LinkNet is a CNN architecture used for semantic segmentation tasks, such as identifying objects or classes in images. It can be used to identify nutrient deficiency in paddy leaf images by dividing the image into different regions. The model incorporates convolutional layers, pooling layers, and transposed convolutional layers, with enhancements in the encoder block and decoder block to ensure consistency. Convolutional layers extract features, pooling layers reduce spatial dimensions, and transposed convolution layers increase spatial resolution.

Figure 6 presents the pictorial representation of Improved LinkNet architecture, including its proposed encoder and decoder blocks as depicted in **Figure 4** and **Figure 5**

1) Proposed Encoder Block:

The Improved LinkNet[17] model uses a sequence of layers to extract hierarchical features from an input feature map. Batch normalization standardizes activations, while convolutional layers convolve the map with learnable filters. An improved ReLU activation function introduces non-linearity and improves gradient flow. Batch normalization enhances network stability. Scale dot product enhances feature representation and discrimination. The improved ReLU activation function learns more complex data relationships. Finally, batch normalization standardizes activations before passing the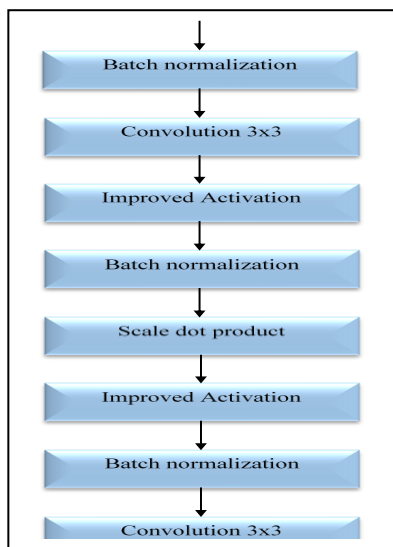m to the next stage. This sequence enhances the network's ability to identify nutrient deficiency. Figure 4 illustrates the proposed encoder block

2) Proposed Decoder Block:

The proposed decoder block upsamples features retrieved from an encoder block and generates the final identification task. It consists of three convolution layers, batch normalization, improved ReLU activation function, and scale dot product. The input feature map undergoes several operations for upsampling and refinement, including convolutional layer, batch normalization, improved activation function, scale dot product, convolutional layer, batch normalization, and convolutional layer for refined segmentation mask. .Figure 5 represents the proposed decoder block
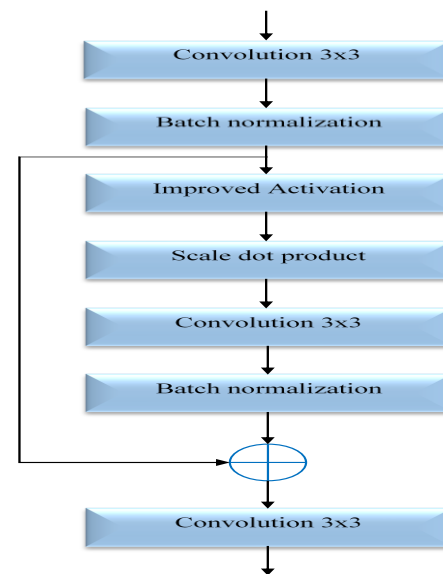

Fig 4. Proposed Encoder Block
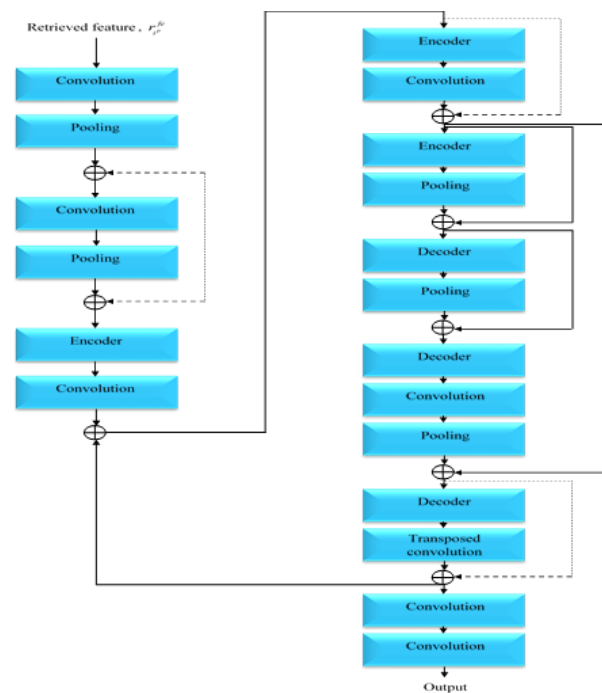

Fig 5. Proposed Decoder Block

Fig 6: Improved LinkNet Architecture

3) Improved Activation function

ReLU is a popular activation function in CNNs because of its simplicity and effectiveness in training deep NN [12] [13]. It changes all negative values in the input with zero, while leaving positive values unchanged. It introduces a slight modification to the standard ReLU function by adding a small positive constant to the negative part of the input. Mathematically, the conventional ReLU activation function can be described as Eq. (14).

$$f(x) = \begin{cases} r_{i^p}^{fe} & if \ r_{i^p}^{fe} \geq 0 \\ 0 & if \ r_{i^p}^{fe} < 0 \end{cases}$$

(14)

$$f(x)_{new} = \begin{cases} r_{i^p}^{fe} & if \ r_{i^p}^{fe} > 0 \\ \dfrac{x}{|x|+1} & if \ 0 > r_{i^p}^{fe} \geq -1 \\ 0 & if \ r_{i^p}^{fe} < 0 \end{cases}$$

(15)

Hence, the improved ReLU activation function is expressed in Eq. (16).

$$AF_{new} = \left\{ \left[\frac{\exp(r_{i^p}^{fe})}{\sum_j \exp(r_{i^p}^{fe})} \right] * \left[f(x)_{new} \right] \right\}$$

(16)

Thus, the proposed model has gradients that do not vanish as quickly as those with traditional activation functions. This leads to faster convergence during training, as the model can learn more efficiently. Additionally, it reduces overfitting, resulting in a performance boost in metrics such as accuracy and precision. It also enhances stability. Therefore, the outcome achieved from this stage is represented as, $ILinkNet^{i^p}$.

3.4.2. SqueezeNet

SqueezeNet [26] stands out among DNN architectures for its unique design, incorporating convolutional layers, max pooling layers, and innovative fire modules as depict in **Figure 10.** Initially, convolutional layers analyze input retrieved feature $r_{i^p}^{fe}$, identifying key patterns relevant to nutrient deficiency detection. Max pooling layers then restructure the feature maps, reducing computational load while maintaining effectiveness. Central to SqueezeNet are its fire modules, which intelligently combine spatial and channel-wise feature reduction, producing concise illustrations of input features. These modules are iterated, facilitating the learning of increasingly intricate feature hierarchies. Following convolutional and fire modules, global average pooling synthesizes feature maps across spatial dimensions, distilling essential information into a compact form. Ultimately, the softmax classifier delivers probabilistic predictions, generating a probability distribution for potential nutrient deficiencies in paddy leaves. Thus, the SqueezeNet output $SqueezeNet^{i^p}$ offers valuable insights, aiding in agricultural diagnosis and management.

Thus, the ILink-SqueezeNet model efficiently identifies the nutrient deficiency via paddy leaf images. Therefore, the model's outputs for nutrient deficiency identification indicate the the Nitrogen as (0), Phosphorous as (1) or Potassium as (2). These outcomes are represented as $ILink - SqueezeNet^{i^p}$.
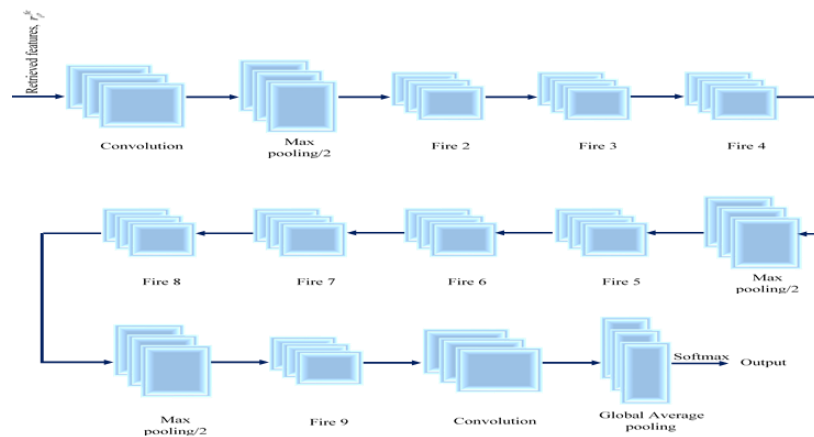

Fig 10: Architecture of the SqueezeNet model

4 Results and Discussion

The dataset used for the experiment is nutrientdeficiencysymptomsinrice[32]

4.1 Performance Analysis

A thorough evaluation was undertaken to assess the efficacy of both ILink-SqueezeNet and traditional methodologies in identifying nutrient deficiencies. This estimation encompassed various vital measures, such as "Sensitivity, False Negative Rate (FNR), Negative Predictive Value (NPV), Specificity, F-measure, Precision, False Positive Rate (FPR), Matthews Correlation Coefficient (MCC), and Accuracy." The ILink-SqueezeNet approach was compared against state-of-the-art techniques such as DNN [7] and LSTM-RNN [8], as well as traditional classifiers including EfficientNet, LinkNet, SqueezeNet, and ResNet. Both the ILink-SqueezeNet and existing approaches were rigorously tested using the Nutrient-Deficiency-Symptoms-in-Rice dataset.

The ILink-SqueezeNet strategy is a leading approach in nutrient deficiency identification, outperforming established models like EfficientNet, LinkNet, LSTM-RNN, DNN, SqueezeNet, and ResNet. The ILink-SqueezeNet method consistently outperforms these models, with accuracy scores rising from 0.865 to 0.966. It also surpasses all existing methodologies in terms of sensitivity, with a sensitivity of 0.796 at 60% training data. As training data increases to 70%, 80%, and 90%, the dominance of the ILink-SqueezeNet strategy becomes increasingly evident, with sensitivity scores reaching remarkable levels of 0.845, 0.885, and 0.941, respectively.

The ILink-SqueezeNet strategy outperforms conventional methods in nutrient deficiency identification by achieving a specificity value of 0.925, surpassing other models like EfficientNet, LinkNet, LSTM-RNN, DNN, SqueezeNet, and ResNet. This high specificity indicates its ability to distinguish healthy samples from deficient ones, minimizing false positives. Other models, like EfficientNet, LinkNet, LSTM-RNN, and ResNet, show similar precisions. The ILink-SqueezeNet approach's superiority can be attributed to its innovative techniques like I-BIRCH, Improved MRE-LBP, and Hybrid model.
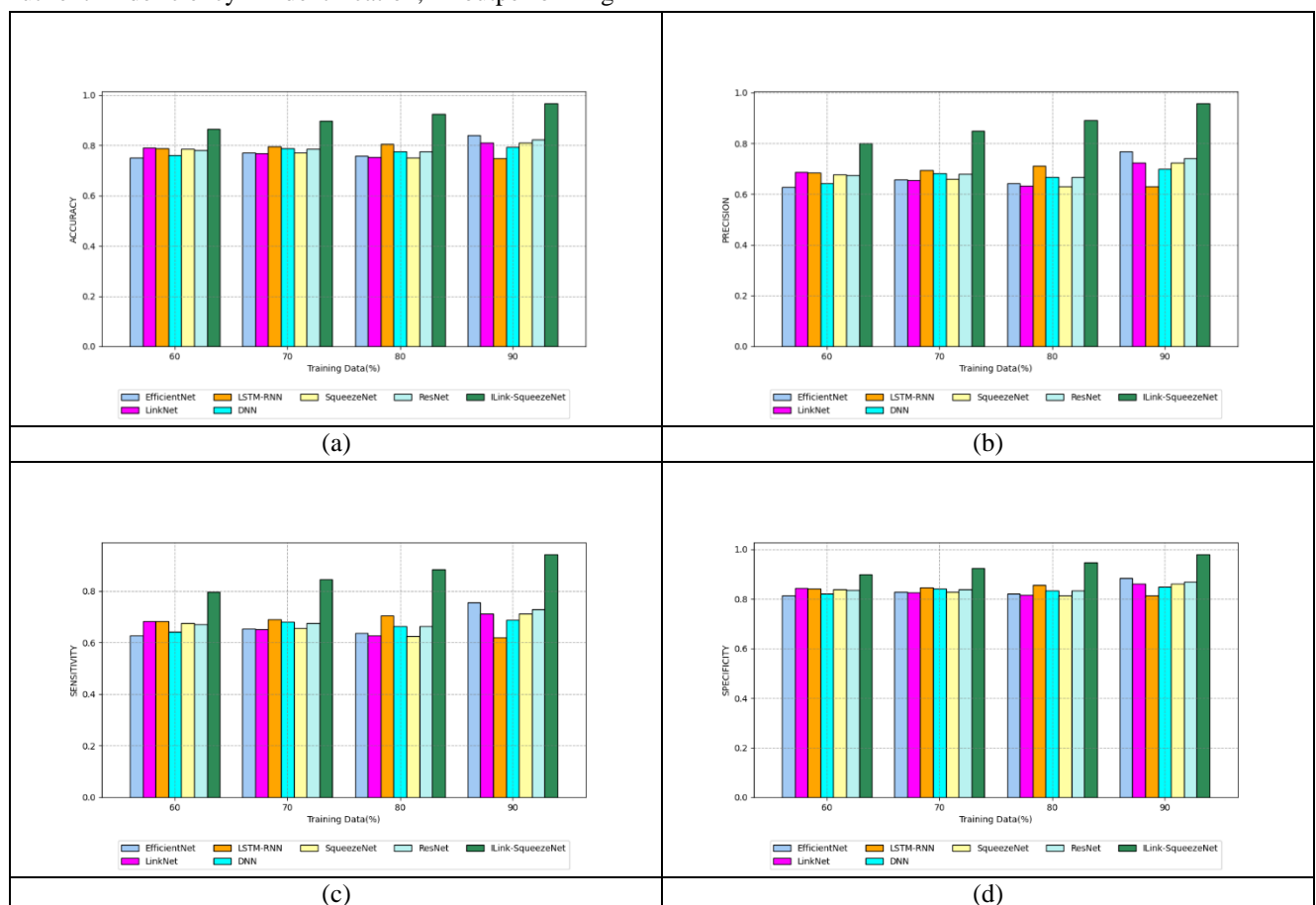

Fig 12 Comparison of Performance Analysis between ILink-SqueezeNet and Conventional Methods

5. Conclusion

In summary, the study presented a comprehensive method that involved several stages, including pre-processing, segmentation, feature extraction, and identification of nutrient deficiencies. Initially, the input paddy leaf image underwent pre-processing via Gaussian filtering technique. Then, the preprocessed image underwent segmentation via I-BIRCH for segmenting the deficient areas. The segmented image then proceeded to the feature extraction stage, where numerous relevant features like

color features, hierarchy of skeleton-based features, and Improved MRE-LBP based features were retrieved. Finally, a hybrid identification model, employing Improved LinkNet and SqueezeNet was utilized to identify the nutrient deficiency. Eventually, the efficacy of this method was assessed, affirming its efficiency in precisely predicting nutrient deficiencies in paddy leaves. Especially, the ILink-SqueezeNet strategy consistently surpassed all other models across all training data percentages, with accuracy scores steadily increasing from 0.865 to an impressive 0.966.

References

[1] Rani, A.P.A.S. and Singh, N.S., "Protecting the environment from pollution through early detection of infections on crops using the deep belief network in paddy". Total Environment Research Themes, Vol.3, p.100020,2022 Dec 1, DOI:https://doi.org/10.1016/j.totert.2022.100020

[2] Liao, F., Feng, X., Li, Z., Wang, D., Xu, C., Chu, G., Ma, H., Yao, Q. and Chen, S., "A hybrid CNN-LSTM model for diagnosing rice nutrient levels at the rice panicle initiation stage". Journal of Integrative Agriculture, Vol.23, Issue.2, pp.711-723, 2024 Feb 1, DOI:https://doi.org/10.1016/j.jia.2023.05.032

[3] Nayak, A., Chakraborty, S. and Swain, D.K., "Application of smartphone-image processing and transfer learning for rice disease and nutrient deficiency detection". Smart Agricultural Technology, Vol.4, p.100195, 2023 Aug 1, DOI:https://doi.org/10.1016/j.atech.2023.100195

[4] Talukder, M.S.H. and Sarkar, A.K., "Nutrients deficiency diagnosis of rice crop by weighted average ensemble learning". Smart Agricultural Technology, Vol.4, p.100155, 2023 Aug 1, DOI:https://doi.org/10.1016/j.atech.2022.100155

[5] Sethy, P.K., Barpanda, N.K., Rath, A.K. and Behera, S.K., "Nitrogen deficiency prediction of rice crop based on convolutional neural network". Journal of Ambient Intelligence and Humanized Computing, Vol.11, pp.5703-5711, 2020 Nov, DOI:https://doi.org/10.1007/s12652-020-01938-8

[6] Shi, P., Wang, Y., Xu, J., Zhao, Y., Yang, B., Yuan, Z. and Sun, Q., "Rice nitrogen nutrition estimation with RGB images and machine learning methods". Computers and Electronics in Agriculture, Vol.180, p.105860, DOI:https://doi.org/10.1016/j.compag.2020.105860

[7] Kolhar, S., Jagtap, J. and Shastri, R., "Deep Neural Networks for Classifying Nutrient Deficiencies in Rice Plants Using Leaf Images". International Journal of Computing and Digital Systems, Vol.16, Issue.1, pp.305-314,2024 Feb 8, DOI:http://dx.doi.org/10.12785/ijcds/160124

[8] Chore, A. and Thankachan, D., "Nutrient defect detection in plant leaf imaging analysis using incremental learning approach with multifrequency visible light approach". Journal of Electrical Engineering & Technology, Vol.18, Issue.2, pp.1369-1387, 2023 March, DOI:https://doi.org/10.1007/s42835-022-01254-5

[9] Sharma, M., Nath, K., Sharma, R.K., Kumar, C.J. and Chaudhary, A., "Ensemble averaging of transfer learning models for identification of nutritional deficiency in rice plant". Electronics, Vol.11, Issue.1, p.148, 2022 Jan 4, DOI:https://doi.org/10.3390/electronics11010148

[10] Xu, Z., Guo, X., Zhu, A., He, X., Zhao, X., Han, Y. and Subedi, R., "Using deep convolutional neural networks for image-based diagnosis of nutrient deficiencies in rice". Computational Intelligence and Neuroscience, Vol.2020, 2020 Aug 8, DOI:https://doi.org/10.1155/2020/7307252

[11] Sobhana, M., Vallabhaneni, R.S., Vasireddy, T. and Polavarpu, D., "Deep Ensemble Mobile Application for Recommendation of Fertilizer Based on Nutrient Deficiency in Rice Plants Using Transfer Learning Models". Int. J. Interact. Mob. Technol., Vol.16, Issue.16, pp.100-112, 2022 Aug 15.

[12] GuiFang Lin, Wei Shen," Research on Convolutional Neural Network based on Improved Relu piecewise activation function" ,Procedia Computer Science ,Volume 131, 2018, Pages 977-984

[13] AF Agarap-arxiv preprint arXiv .1803.08375, https://doi.org/10.48550/arXiv.1803.08375

[14] Sara, L., Saeheng, S., Puttarak, P. and Klinnawee, L., "Changes in Metabolites and Allelopathic Effects of Non-pigmented and Black-pigmented Lowland indica Rice Varieties in Phosphorus Deficiency" Rice Science, 2024 March 1, DOI:https://doi.org/10.1016/j.rsci.2024.02.009

[15] Simhadri, C.G. and Kondaveeti, H.K., "Automatic recognition of rice leaf diseases using transfer learning". Agronomy, Vol.13, Issue.4, p.961, 2023 march 23, DOI:https://doi.org/10.3390/agronomy13040961

[16] Taha, M.F., Abdalla, A., ElMasry, G., Gouda, M., Zhou, L., Zhao, N., Liang, N., Niu, Z., Hassanein, A., Al-Rejaie, S. and He, Y., "Using deep convolutional neural network for image-based diagnosis of nutrient deficiencies in plants grown in aquaponics". Chemosensors, Vol.10, Issue.2, p.45, DOI:https://doi.org/10.3390/chemosensors10020045.

[17] Ruba, M.T., Tamilselvi, R., Beham, M.P. and Gayathri, M., "Segmentation of a Brain Tumour using Modified LinkNet Architecture from MRI

Images". Journal of Innovative Image Processing, Vol.5, Issue.2, pp.161-180.

[18] Sharma, M., Kumar, C.J., Talukdar, J., Singh, T.P., Dhiman, G. and Sharma, A., "Identification of rice leaf diseases and deficiency disorders using a novel DeepBatch technique". Open Life Sciences, Vol.18, Issue.1, p.20220689, 2023 Aug 28.

[19] Sivagami, S. and Mohanapriya, D., "Hybrid Method for Detection and Classification of Paddy leaf Deficiency Using Modified K-Means Image Segmentation". Indian Journal of Computer Science and Engineering (IJCSE), Vol. 11, Issue. 6 Nov-Dec 2020, DOI : 10.21817/indjcse/2020/v11i6/201106010

[20] Ghorai, A.K., Mukhopadhyay, S., Kundu, S., Mandal, S., Barman, A.R., De Roy, M. and Dutta, S., "Image processing based detection of diseases and nutrient deficiencies in plants". SATSA Mukhapatra, Vol.25, Issue.1, pp.1-24, Jan 28 2021.

[21] Vishal, M.K., Saluja, R., Aggrawal, D., Banerjee, B., Raju, D., Kumar, S., Chinnusamy, V., Sahoo, R.N. and Adinarayana, J., "Leaf Count Aided Novel Framework for Rice (Oryza sativa L.) Genotypes Discrimination in Phenomics: Leveraging Computer Vision and Deep Learning Applications". Plants, Vol.11, Issue.19, p.2663, 2022 Oct 10, DOI:https://doi.org/10.3390/plants11192663

[22] Azimi, S., Kaur, T. and Gandhi, T.K., "A deep learning approach to measure stress level in plants due to Nitrogen deficiency". Measurement, Vol.173, p.108650, 2021 March 1, DOI:https://doi.org/10.1016/j.measurement.2020.108650

[23] Yi, J., Krusenbaum, L., Unger, P., Hüging, H., Seidel, S.J., Schaaf, G. and Gall, J., "Deep learning for non-invasive diagnosis of nutrient deficiencies in sugar beet using RGB images". Sensors, Vol.20, Issue.20, p.5893, 2020 Oct 18, DOI:https://doi.org/10.3390/s20205893

[24] Ali, A., Ali, S., Husnain, M., Saad Missen, M.M., Samad, A. and Khan, M., "Detection of deficiency of nutrients in grape leaves using deep network". Mathematical Problems in Engineering, 2022 Jan 31, DOI:https://doi.org/10.1155/2022/3114525

[25] Lewis, K.P. and Espineli, J.D., "Classification and detection of nutritional deficiencies in coffee plants using image processing and convolutional neural network (Cnn)". Int. J. Sci. Technol. Res, Vol.9, Issue.4, pp.2076-2081, 2020 April.

[26] Bernardo, L.S., Damaševičius, R., Ling, S.H., de Albuquerque, V.H.C. and Tavares, J.M.R., "Modified SqueezeNet architecture for Parkinson's disease detection based on keypress data". Biomedicines, Vol.10, Issue.11, p.2746.

[27] Hoque, N., Bhattacharyya, D.K. and Kalita, J.K., "MIFS-ND: A mutual information-based feature selection method". Expert systems with applications, Vol.41, Issue.14, pp.6371-6385, 2014 Oct 15,DOI:https://doi.org/10.1016/j.eswa.2014.04.019

[28] Wilson, D.R. and Martinez, T.R., "Improved heterogeneous distance functions". Journal of artificial intelligence research, Vol.6, pp.1-34,1997 Jan 1.

[29] Zenggang, X., Zhiwen, T., Xiaowen, C., Xue-min, Z., Kaibin, Z. and Conghuan, Y., "Research on image retrieval algorithm based on combination of color and shape features". Journal of signal processing systems, Vol.93, pp.139-146, DOI:https://doi.org/10.1007/s11265-019-01508-y

[30] Ayzenberg, V. and Lourenco, S.F., "Skeletal descriptions of shape provide unique perceptual information for object recognition". Scientific reports, Vol.9, Issue.1, p.9359, DOI:https://doi.org/10.1038/s41598-019-45268-y

[31] L. Liu, S. Lao, P. W. Fieguth, Y. Guo, X. Wang and M. Pietikäinen, "Median Robust Extended Local Binary Pattern for Texture Classification," in IEEE Transactions on Image Processing, vol. 25, no. 3, pp. 1368-1381, March 2016, doi: 10.1109/TIP.2016.2522378.

[32] https://www.kaggle.com/datasets/guy007/nutrientdeficiencysymptomsinrice